Available online at www.sciencedirect.com

ScienceDirect

Procedia Engineering 116 (2015) 221 – 228

Procedia Engineering

www.elsevier.com/locate/procedia

8th International Conference on Asian and Pacific Coast (APAC 2015)

Design of a numerical wave tank and wave flume for low steepness waves in deep and intermediate water

Shaswat Saincher[a], Jyotirmay Banerjee[a,*]

[a]*Mechanical Engineering Department, S. V. National Institute of Technology, Surat 395007, India*

Abstract

Understanding the dynamics of wave energy converters and vortical structure of breaking waves are challenging hydrodynamic problems relevant to coastal engineering. These issues can be addressed at the laboratory scale through a specialized class of devices known as experimental wave flumes and numerical wave tanks (NWTs). This paper presents the process of design and development of a NWT and a wave flume that would eventually be applied for analyzing the hydrodynamics of breaking waves. The wave characteristics to be simulated have been selected from literature based on measurements carried out in the Gulf of Kutch, Gujarat. The NWT is based on a volume-of-fluid (VOF) formulation of the Navier-Stokes equations on a staggered grid using the mass-source function technique for wave generation. The flume is an acrylic tank equipped with a flap type wavemaker having dimensions adopted from the NWT. It is demonstrated in this work that the NWT and flume accurately generate non-linear wave trains in both intermediate as well as deep water with steepness $H/\lambda \sim 0.04$.

Peer- Review under responsibility of organizing committee , IIT Madras , and International Steering Committee of APAC 2015

Keywords: Waves; flume; numerical wave tank; simulation; non-linear

1. Introduction

Transport processes occurring at the atmosphere-ocean interface (such as gas exchange, salt ejection, wind-induced momentum addition etc.) are crucial to the operation of various ecological cycles and, thus, to the survival of life on Earth. As the air-sea interface is deformable (being susceptible to tangential stresses), these transport processes are characterized by (omnipresent) wave propagation. The latter plays a pivotal role in sustenance of air-sea interaction through the hydrodynamic mechanisms of macroscale and microscale wave breaking. In addition, ocean waves represent the most concentrated form of renewable energy available on Earth, generating a strong motivation for technological development towards harnessing of this energy source. To address these challenging issues pertaining to

*Corresponding author. Tel.: +91 261 2204145; fax: +91 261 2228394.
E-mail address: jbaner@med.svnit.ac.in

Peer- Review under responsibility of organizing committee , IIT Madras , and International Steering Committee of APAC 2015
doi:10.1016/j.proeng.2015.08.394

coastal engineering, there is a need to replicate ocean wave propagation conditions in the laboratory. Devices commonly used for this purpose are called *wave tanks* which can be further categorized into numerical wave tanks (NWTs) and experimental wave flumes. The design of wave tanks should be such that the following operational requirements are fulfilled; (a) *generation of waves from one end of the tank*, (b) *restriction of reflections from the opposite end* and (c) *attainment of desired wave characteristics with an acceptable level of accuracy*. Simultaneous attainment of these requirements has proved to be a challenging task and has motivated contemporary research towards development of more robust flume and NWT designs.

A *wave flume* is a physical tank, having length significantly larger than the cross-sectional dimensions, for the generation of two-dimensional waves trains. A *wavemaker* is used to periodically agitate water from one end of the flume and a dissipating *beach* restricts energetic reflections from the opposite end. The characteristics of the wave train (such as period T and height H) are correlated to the motion of the wave generator through *wavemaker theory* (WMT) [1,2]. Although a variety of wave generators have been designed for flumes [2], the *piston* [3] and *flap* [4] type wavemakers have found extensive application in coastal engineering research. These wavemakers have been known to perform accurately for small-steepness waves [5,6]. However, attainment of a target wave height using piston or flap type wavemakers becomes difficult as the wave steepness increases [5,6]. It has been recently speculated [6] that this discrepancy (in wave height) between theory and experiments may be related to an increase in wave celerity (C) for steep waves.

A *numerical wave tank* is the computational counterpart of the wave flume. In a NWT, the wave propagation is simulated either by a velocity potential (ϕ) approach [7,8] or a Navier-Stokes equation model (NSEM) [6,9]. A NWT model usually comprises of a wave generator at one end and an artificial beach or porous region (sponge layer) at the other end to restrict reflections. In fact, wave generation and absorption in a NWT can also be handled by appropriate *inflow* and *outflow* (radiation) [9] boundary conditions. The design of NWTs has undergone substantial improvement over the past three decades. However, in case of both velocity potential-based and NSEM-based NWTs, contemporary formulations do not exhibit the same level of accuracy for all cases of wave generation. This has been found to especially be the case for steep and deep water waves [6,8,10].

The present work deals with the design and development of a NWT and wave flume for generation of non-linear (regular) wave trains in deep and intermediate water. The wave tanks have been sized based on dynamic scaling of wave measurements carried out in the Gulf of Kutch, Gujarat [11]. The NWT is a Navier-Stokes based numerical tank in which the wave propagation is treated as two-phase flow on a staggered grid. The mass-source function technique has been used for wave generation [9] and a combination of sponge layers [10] and Sommerfeld (radiation) boundaries [9] has been used for preventing energetic reflections. Based on the dimensions of NWT, an acrylic flume has been developed that employs a flap-type wavemaker for wave generation. An adjustable beach is used on the opposite end to effectively dissipate incoming wave energy. The wave generation performance of the NWT and flume have been compared with `Stokes` wave theory and wavemaker theory (WMT) respectively. It is demonstrated that both tanks accurately simulate deep and intermediate water wave propagation conditions.

2. Wave tank design

The selection of dimensions and components of a wave tank is dictated by the nature of the waveform that is to be simulated. The procedure of designing the NWT and wave flume for a target wave propagation application is discussed in detail in the present section.

2.1. Wave characteristics and scaling criteria

Wave characteristics, that are to be simulated in the wave tanks, have been developed by dynamically scaling measurements made in 15 m deep water at Hansthal creek in the Gulf of Kutch, Gujarat [11]. The same are shown in table 1. As the wave tanks are to be modeled for deep and intermediate water, the wave dynamics would fall within the range of short wave behavior. For short waves, a maximum scaling factor of $\mathcal{L} = 50$ is permissible [2]. Considering this scaling limit, the wave characteristics designed for simulation are shown in table 2. It should be noted that dynamic similitude has been maintained between the wave conditions in the Gulf and the laboratory. This means the wave characteristics having the dimensions of length have been scaled by $\mathcal{L}$ while those having the dimensions of

Table 1. Wave data in the Gulf of Kutch [11]

Month	H_s range	T range
June-July	$0.5\,m - 1.5\,m$	$3\,s - 6\,s$
August-October	$0.5\,m - 1.5\,m$	$2\,s - 6\,s$
November-February	$0.5\,m - 1.0\,m$	$3\,s - 16\,s$
April	$0.5\,m - 2.5\,m$	$3\,s - 15\,s$

time have been scaled by $\sqrt{\mathcal{L}}$. Such a scaling methodology ensures that the Froude (Fr), Strouhal (St) and Euler (Eu) numbers attained in the wave tank are equal to those in the Gulf of Kutch [2,12]. The designs of the NWT and flume are presented in the following subsections.

Table 2. Dynamically scaled wave characteristics for simulation

		$\lambda\,(m)$	$h\,(m)$	$H\,(m)$	$T\,(s)$
Intermediate water $\mathcal{L} = 50$	Gulf of Kutch	37.75	15.0	1.5	4.95
	Wave tank	0.755	0.3	0.03	0.7
Deep water $\mathcal{L} = 30$	Gulf of Kutch	22.95	15.0	0.9	3.83
	Wave tank	0.765	0.5	0.03	0.7

2.2. Numerical wave tank (NWT)

Based on the wave characteristics proposed in table 2, a computational model is developed for the NWT which is shown in figure 1. The wave propagation problem has been modeled as two-phase flow on a staggered grid using Young's PLIC-VOF technique [13]. The dimensional set of two-phase Navier-Stokes equations used for simulation of wave propagation are represented by the set of equations (1).

$$\begin{aligned}
&\iint_{CS} \vec{V} \bullet d\vec{A} = 0 \\
&\iiint_{C\forall} \frac{\partial U}{\partial t} d\forall + \iint_{CS} \left(U\vec{V}\right) \bullet d\vec{A} = -\frac{1}{\rho^*} \iiint_{C\forall} \frac{\partial p}{\partial x} d\forall + \frac{1}{\rho^*} \iint_{CS} \left(\mu^* \vec{\nabla} U\right) \bullet d\vec{A} \\
&\iiint_{C\forall} \frac{\partial V}{\partial t} d\forall + \iint_{CS} \left(V\vec{V}\right) \bullet d\vec{A} = -\frac{1}{\rho^*} \iiint_{C\forall} \frac{\partial p}{\partial y} d\forall + \frac{1}{\rho^*} \iint_{CS} \left(\mu^* \vec{\nabla} V\right) \bullet d\vec{A} - \iiint_{C\forall} g d\forall
\end{aligned} \tag{1}$$

Here, U and V denote the streamwise and vertical components of velocity, p is the pressure, ρ^* and μ^* are the mixture density and mixture viscosity, g is the acceleration due to gravity and $d\vec{A}$ and $d\forall$ represent differential area and volume of integration for a finite volume discretization. The mixture properties are calculated as,

$$\rho^* = f\rho_w + (1-f)\rho_a \;\text{ and }\; \mu^* = f\mu_w + (1-f)\mu_a \tag{2}$$

where subscripts w and a denote the water and air phases respectively and f is the volume fraction. A semi-explicit Navier-Stokes solver has been used for solution of equation set (1). The wave simulation region of the NWT is $6\,m \times 1\,m$ and is situated within the range $4\,m \le x \le 10\,m$. No energy damping is imposed within the simulation region. Outside the simulation region, two $4\,m$ long sponge layers are modeled at either end. The west sponge layer induces energy damping through a combination of velocity damping ($V-$component) [14] and grid stretching ($x-$direction). The east sponge layer uses grid stretching and a Sommerfeld boundary to prevent unwanted reflections.

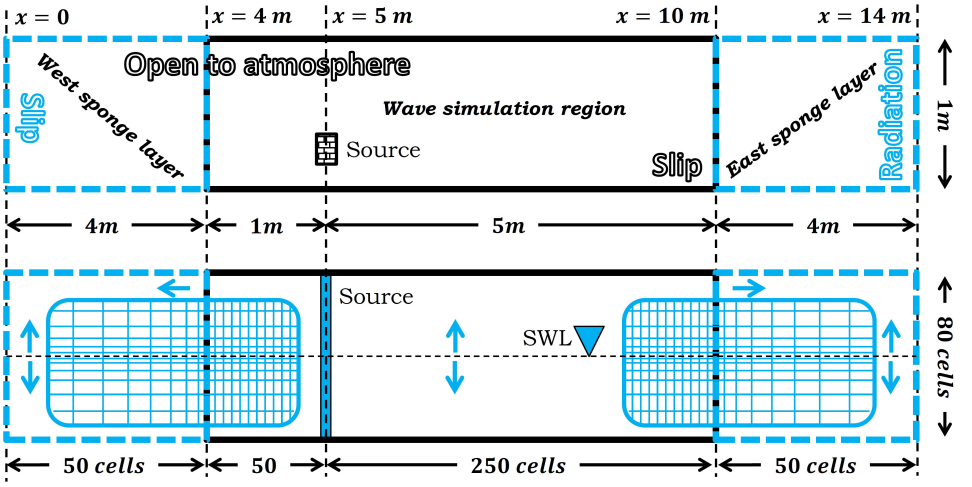

Fig. 1. *Computational model of the NWT showing source location and boundary conditions. Blue arrows indicate the direction of grid stretching.*

A mass source-based wave generator has been initialized as a single-cell thick region within the water phase. Within the source region, the equation of continuity (EOC) is modified as,

$$\iint_{CS} \vec{V} \bullet d\vec{A} = \iiint_{C\forall} s(t) d\forall \tag{3}$$

where $s(t)$ is the strength of the source. The height of the source region lies in the range $h/7 \sim h/6$ while the distance of the source center from the still water level (SWL) lies within the range $h/6 \sim h/5$. The wave designs listed in table 2 fall within the purview of `Stokes` theory. Hence, the expression of source strength follows the topology of a `Stokes II` wave,

$$s(t) = \frac{\lambda H}{A_s T} \sin(\omega t) - \frac{\lambda H^2 k}{8 A_s T} \frac{\cosh(kh)\,(2 + \cosh(2kh))}{\sinh^3(kh)} \cos(2\omega t) \tag{4}$$

where, A_s is the area of the source region, k is the circular wavenumber, ω is the circular frequency and t is time. A 401×80 non-uniform mesh has been used with enhanced resolution near the SWL to accurately resolve the energy content within the crests and troughs. Based on this NWT configuration, a wave flume has been designed and fabricated. This is discussed in detail in the next subsection.

2.3. Wave flume

The flume serves as a three-dimensional realization of the simulation region of the NWT and is shown in figure 2. It is a $6.0\,m \times 0.6\,m \times 1.0\,m$ acrylic tank with the wavemaker situated $1.0\,m$ away from the end opposite to the beach. The tank has been fabricated as a modular structure comprising of one $1.2\,m$ long and two $2.4\,m$ long sections. The beach is $3\,m$ in length with the toe of the beach $2\,m$ away from the wavemaker. As the wave characteristics have been designed for deep and intermediate water, a paddle type wavemaker with a flap motion has been used for agitating water. The flap is driven by a $2\,hp$ gear motor having a constant torque output with a $6:1$ speed reduction. The speed reduction ensures the availability of a high output torque at the flap to prevent sloshing-induced variations in angular frequency (ω) [12]. Having said that, the angular frequency of the flap can be assumed to be equal to that of the generated waves. Hence, the target wave height (H) can be related to the stroke of the flap (S) by a *height-to-stroke* expression [1],

$$\left[\frac{H}{S}\right]_{\text{flap}} = 4\left(\frac{\sinh(kh)}{kh}\right)\left(\frac{kh\sinh(kh) - \cosh(kh) + 1}{\sinh(2kh) + 2kh}\right) \tag{5}$$

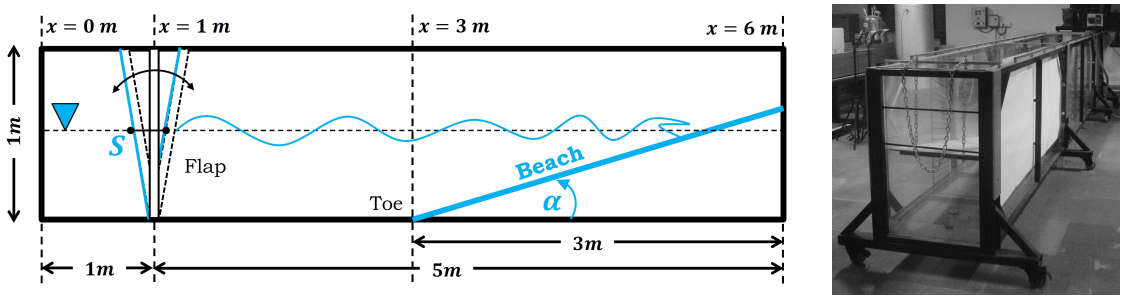

Fig. 2. *The* $6.0\,m \times 0.6\,m \times 1.0\,m$ *wave flume designed and fabricated based upon the NWT dimensions.*

From equation (5), the stroke of the flap (S) required for attaining a target wave height (H) can be obtained for a particular value of the relative water depth (kh). The values of stroke obtained for the present wave design are listed in table 3. The incident wave height at the toe of the beach is measured through high-speed videography of the air-water

Table 3. Design values of wavemaker stroke (S) required for achieving the target wave height (H)

	$H\,(cm)$	kh	H/S	$S\,(cm)$
Intermediate water	3.00	2.50	1.22	2.46
Deep water	3.00	4.11	1.52	2.00

interface against a graduated scale using a Casio Exilim camera at $210\,fps$. The period of the waves is measured as the average time required for the passage of 50 wavelengths past the toe of the beach, using a stopwatch. The wave height and period measurements have been repeated for 20 experimental runs of which the 10 most accurate measurements have been reported here. The next section presents the results of wave generation obtained using the NWT and flume.

3. Results of wave generation and discussion

The wave generation performance of the NWT has been evaluated both qualitatively and quantitatively. In a qualitative sense, numerical results are compared with analytic solutions for (a) spatial topology, (b) wave envelopes and (c) orbital motion of water particles beneath the waves. Figure 3 shows the development of the spatial topology of the waves in intermediate and deep water. The simulations have been run for 21 wave periods. A unique feature of the NWT formulation is that the water phase has been visualized by plotting the geometrically reconstructed interface [13]. As the steepness of both designs is nearly identical (the intermediate water wave is only longer by a centimeter), the spatial topologies look similar. Further, a very close match is observed between the source-generated wave profile and the analytic `Stokes` curve. It should be noted that the analytic curve has a wavelength correction incorporated from `Stokes III` theory to account for amplitude dispersion [8]. Figure 4 shows the wave envelopes generated during the last wave period $t = 20T - 21T$ within the simulation region. The numerical envelopes have been obtained by successively plotting the PLIC-VOF generated air-water interface for 10 equi-spaced instances during a wave period. An envelope plot indicates subtle changes in wavelength and wave height occurring during a wave period that are not perceptible through the spatial profiles. It is observable from figure 4 that the intermediate water envelope attains a uniform topology away from the source region and achieves a close resemblance to the analytic envelope. This indicates that, even after a passage of 21 wave periods, inward reflections occurring from the sponge layers are minimal and have a negligible effect on the wave topology.

This is however not true in case of the deep water envelope. The deep water envelope shows small undulations that are indicative of fluctuations in wave height caused by reflections from the east sponge layer. Figure 5 shows another unique feature of the present NWT in that a MAC-like particle tracking routine has been used to generate numerical visualizations of orbital motion of water particles beneath the waves. The particles have been released at

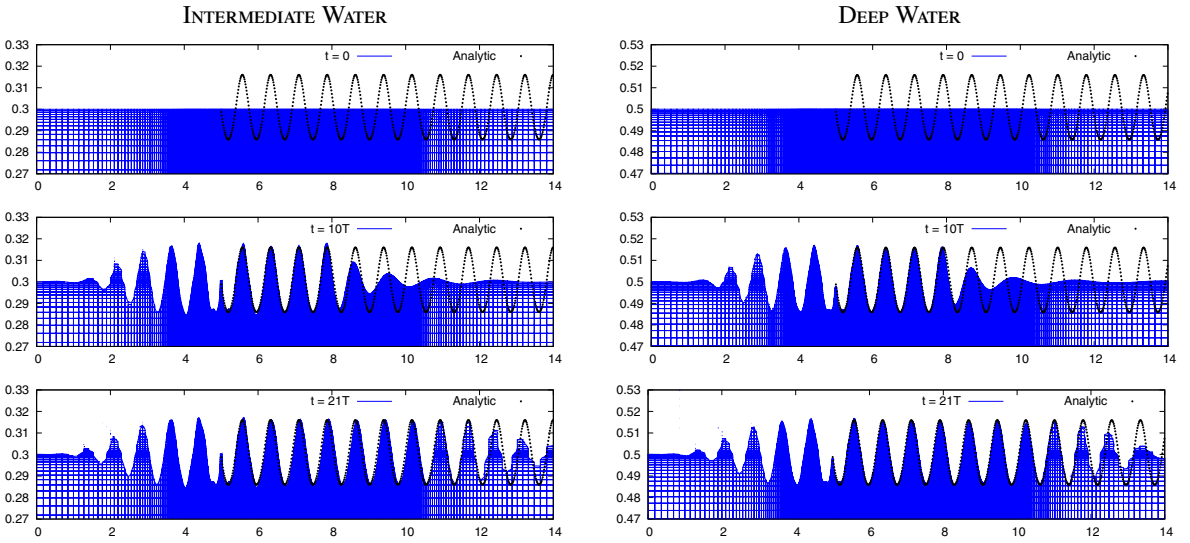

Fig. 3. *Time evolution of the spatial profile of the waves superimposed by the analytic* `Stokes III` *solution.*

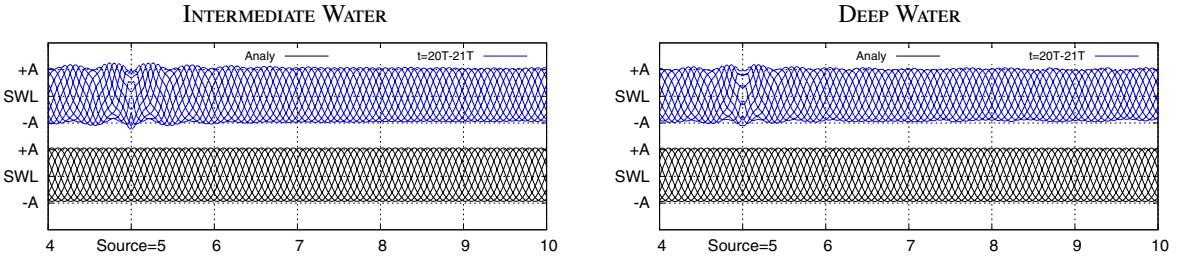

Fig. 4. *Wave envelopes generated during the last wave period* $(20T - 21T)$ *compared with the* `Stokes III` *solution.*

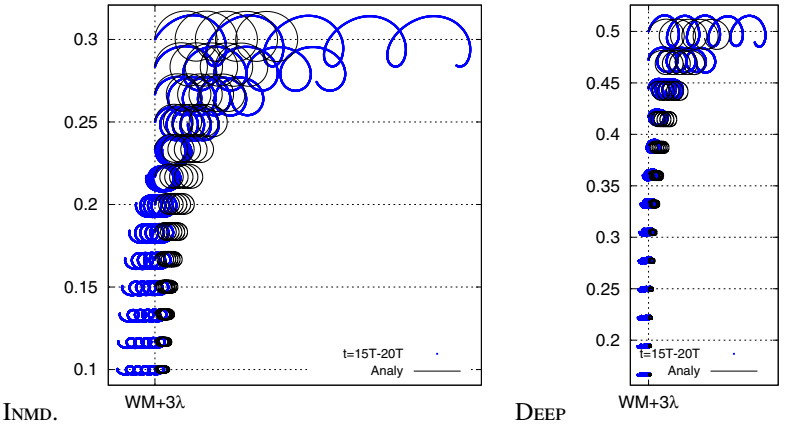

Fig. 5. *Particle motion visualized at a distance of* $+3\lambda$ *from the wavemaker (WM) in* $h/3 \leq y \leq h$ *for five periods* $(t = 15T - 20T)$*. The* **blue lines** *indicate trajectories generated using the numerical velocity field while the* **black lines** *indicate those generated using an analytic* `Stokes` *field.*

13 equi-spaced locations within the top two-thirds of the water depth and advanced in time for five wave periods. It can be observed (from figure 5) that the numerical trajectories exhibit the correct rate of decay of orbital amplitude

in intermediate and deep water; the rate of decay is greater in deep water. Midway through the water depth, the numerical trajectories appear to propagate in the opposite direction. This indicates the presence of a returning current from the east sponge layer towards the wave generator. The wave generation performance of the NWT has been quantitatively summarized in table 4. Four parameters have been defined for this purpose; (a) the percentage change

Table 4. Quantitative evaluation of wave generation performance of the NWT after 21 wave periods

	$\mathcal{VE}(\%)$	$\mathcal{HE}(\%)$	$\mathcal{WE}(\%)$	$\mathcal{CT}(s)$
Intermediate water	+0.13	+2.50	+0.77	1729.37
Deep water	+0.06	−2.00	+0.41	1371.50

in water volume ($\mathcal{VE}$), (b) the percentage error in H ($\mathcal{HE}$) at $x = 7\,m$, (c) the percentage error in λ ($\mathcal{WE}$) at $x = 7\,m$ and (d) computational time in seconds ($\mathcal{CT}$) after 21 wave periods. It can be seen from table 4 that the volume of water fluctuates by a negligible amount. Further, there is a slight under-prediction of H due to reflections in deep water. The percentage error in λ is however observed to be lower than that in H. The wave generation performance of the flume has been quantitatively evaluated from the standpoint of two parameters; (a) $\mathcal{HE}$ and (b) $\mathcal{WE}$. As mentioned previously, the 10 most accurate runs of the flume have been represented in the form of a H/S vs. kh plot in figure 6. These 10 measurements are averaged. The percentage errors $\mathcal{HE}$ and $\mathcal{WE}$ are computed and are tabulated on the right

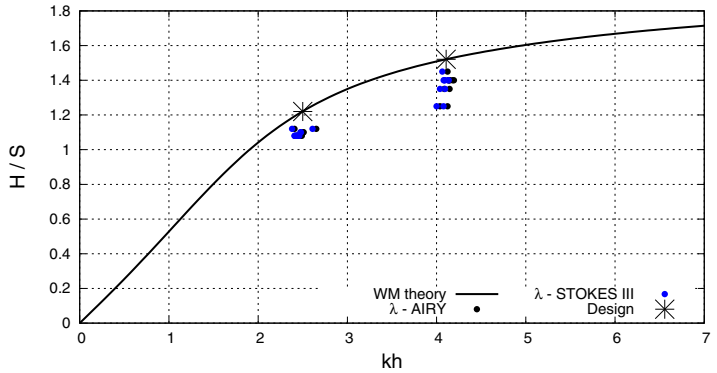

	Intermediate	Deep
Mean $H\,(cm)$	2.73	2.73
Mean $\lambda\,(m)$	0.761	0.761
$\mathcal{HE}(\%)$	−9.00	−9.00
$\mathcal{WE}(\%)$	+0.80	−0.52

Fig. 6. *Experimentally observed values of wave height in intermediate and deep water compared with wavemaker theory. The* **black dots** *indicate data points where the wavelength is obtained using the linear dispersion relation while the* **blue dots** *indicate wavelength corrected using the* `Stokes III` *theory.*

of figure 6. The plotted data indicates an equal amount of scatter in wave period (wavelength) for both wave designs. However, a greater amount of scatter is observable in the wave height in deep water. The scatter in measurements of H in deep water reflect, upto some extent, the challenges that were encountered in achieving repeatability in experimental runs in deep water. As the steepness of the flap-generated waves (H/λ) is almost equivalent in intermediate and deep water, factors leading to the loss of repeatability are not clear at this stage. Further investigation is necessary in this regard. Another important observation that can be made from the plotted data is that if the wavelength is corrected using the third-order dispersion relationship, the values approach closer to the WMT curve [6]. Hence, despite some discrepancies, the NWT and flume are observed to generate non-linear wave trains with sufficient accuracy.

The present NWT model, as stated earlier, is being developed for eventually simulating shoaling and breaking of non-linear wave trains on a beach. The modeling of a sloping beach within the domain necessitates an extension of the NWT model to general coordinates; this is a task that is to be taken up in the immediate future. In this regard, although NWT simulations of breaking are unavailable for analysis at this stage, figure 7 shows high-speed photography of a plunging breaker ($h = 0.4\,m$, $H_o \approx 0.05\,m$, $T_o \approx 0.7\,s$) carried out in the flume. The sequence of images shown in figure 7 depict the following timeline for a plunging breaker; (a) forward ejection of a *jet* from the steepening wave crest; the jet entraps air ahead of the crest → (b) the jet rebounds from the forward face initiating a reactionary

Fig. 7. *The breaking region visualized at* 210 *f ps at a deep-water Iribarren number* ($\Xi_o \equiv \tan\alpha \times \sqrt{\lambda_o/H_o}$) *of* 0.776.

splash-up; deformations appear in the topology of the air cavity → (c) the splash-up reaches maximum height; the cavity becomes completely turbulent → (d) the cavity is detrained of air and collapses completely followed by → (e) the gravitational collapse of the rebounding jet. Future investigation will be targeted towards simulating the breaking phenomenon through the NWT model in general coordinates.

4. Conclusion

A numerical wave tank and a wave flume have been designed and developed for simulation of low steepness waves in intermediate and deep water. The NWT simulations capture the spatial topology and envelope structure of the progressive wave train with sufficient accuracy. However, discrepancies are observed between analytic and numerically visualized water particle motion. This discrepancy arises in the generation of a returning current within the numerical tank from the east sponge layer towards the wavemaker which causes the orbital motion to essentially reverse at the bottom of the NWT. The wave designs simulated numerically have also been generated experimentally in the flume. It has been observed that the wave height is approximately 10% smaller than the design value in both intermediate and deep water. Even though the error in H is consistent with literature [6], factors responsible for it's occurrence need to be identified and eliminated from the design of the flume.

References

[1] R.G. Dean, R.A. Dalrymple, Water wave mechanics for engineers and scientists, Advanced Series on Ocean Engineering–Volume 2. World Scientific Publishing Co. Pte. Ltd., 1991, pp. 41–178.
[2] S.A. Hughes, Physical models and laboratory techniques in coastal engineering, Advanced Series on Ocean Engineering–Volume 7. World Scientific Publishing Co. Pte. Ltd., 1993, pp. 51–356.
[3] D. Stagonas, D. Warbrick, G. Muller, D. Magagna, Surface tension effects on energy dissipation by small scale, experimental breaking waves, Coastal Engineering 58 (2011) 826–836.
[4] J. Belden, A.H. Techet, Simultaneous quantitative flow measurement using PIV on both sides of the airwater interface for breaking waves, Experiments in Fluids 50 (2011) 149–161.
[5] F. Ursell, R.G. Dean, Y.S. Yu, Forced small-amplitude water waves: A comparison of theory and experiment, Journal of Fluid Mechanics 7 (1960) 32–53.
[6] M. Anbarsooz, M. Passandideh-Fard, and M. Moghiman, Fully nonlinear viscous wave generation in numerical wave tanks, Ocean Engineering 59 (2013) 73–85.
[7] M. Brorsen, J. Larsen, Source Generation of Nonlinear Gravity Waves with the Boundary Integral Equation Method, Coastal Engineering 11 (1987) 93–113.
[8] U. Senturk, Modeling non-linear waves in a numerical wave tank with localized meshless RBF method, Computers and Fluids 44 (2011) 221–228.
[9] P. Lin, P.L-F. Liu, Internal Wave-Maker for Navier-Stokes Equations Models, Journal of Waterway, Port, Coastal, and Ocean Engineering 125 (1999) 207–215.
[10] T. Ha, P. Lin, Y-S. Cho, Generation of 3D regular and irregular waves using Navier-Stokes equations model with an internal wave maker, Coastal Engineering 76 (2013) 55–67.
[11] B.U. Nayak, P. Chandramohan, S. Mandal, Evaluation of wave characteristics in the Gulf of Kutch, Gujarat, Indian Journal of Marine Sciences 19 (1990) 83–88.
[12] Y. Liu, G. Cavalier, J. Pastor, R.J. Viera, C. Guillory, K. Judice, K. Guiberteau, T.A. Kozman, Design and construction of a wave generation system to model ocean conditions in the gulf of Mexico, International Journal of Energy & Technology 4 (2012) 1–7.
[13] S. Saincher, J. Banerjee, A redistribution-based volume-preserving PLIC-VOF technique, Numerical Heat Transfer, Part B 67 (2015) 338–362.
[14] Z. Hafsia, M.B. Hadj, H. Lamloumi, K. Maalel, Internal inlet for wave generation and absorption treatment, Coastal Engineering 56 (2009) 951–959.